Basin stability for burst synchronization in small-world networks of chaotic slow-fast oscillators

Oleg V. Maslennikov,[1] Vladimir I. Nekorkin,[1] and Jürgen Kurths[1,2]
[1]*Institute of Applied Physics, Russian Academy of Sciences, 46 Ul'yanov street, 603950, Nizhny Novgorod, Russia*
[2]*Potsdam Institute for Climate Impact Research, Telegraphenberg, D-14415 Potsdam, Germany*
(Received 6 May 2015; revised manuscript received 9 September 2015; published 6 October 2015)

The impact of connectivity and individual dynamics on the basin stability of the burst synchronization regime in small-world networks consisting of chaotic slow-fast oscillators is studied. It is shown that there are rewiring probabilities corresponding to the largest basin stabilities, which uncovers a reason for finding small-world topologies in real neuronal networks. The impact of coupling density and strength as well as the nodal parameters of relaxation or excitability are studied. Dynamic mechanisms are uncovered that most strongly influence basin stability of the burst synchronization regime.

DOI: 10.1103/PhysRevE.92.042803 PACS number(s): 89.75.Fb, 05.45.Xt

I. INTRODUCTION

Collective phenomena in neuronal networks that exhibit bursting oscillations have a particular meaning for understanding many vital processes in brain and cell cultures [1]. Burst oscillations consist of alternating periods of groups of spikes and periods of quiescence. From a nonlinear dynamics viewpoint, such oscillatory mode is a relaxation; i.e., it is characterized by two different time scales, fast and slow. Another dynamic feature that may be inherent to bursting oscillations is their chaotic nature. When analyzing large-scale neural circuits, one usually needs to use concepts and approaches of complex networks theory [2–5] considering these circuits as sets of nodes coupled by links and studying their interaction. One of the important collective effects in neuronal networks exhibiting bursting is burst synchronization, where spiking phases of different neurons start and end at the same (close) moments, while single spikes within bursts appear generally at different moments [6–10] (see also Refs. [11,12]). It was shown in Refs. [13–15] that network mechanisms, i.e., connectivity pattern and coupling strength, are significant for burst synchronization, in particular, in such a class of complex networks as small-world ones. The property of "small-worldness" [16,17] is assumed to be very important in nature, technology, and society due to its universality. Many anatomical and functional networks of various brain areas are confirmed to be small-world and at a first approximation can be described as small-world Watts-Strogatz networks (see, e.g., Refs. [18–20]). It should be noted that the reason was unclear for a long time why real networks have small-world features holding an intermediate position between regular and random ones. Only recently a reason was proposed in Refs. [21,22], namely that small-world oscillatory networks display the largest possible basin stability of the synchronization regime. Basin stability characterizes the relative volume of phase space containing initial conditions starting from which trajectories tend to the attractor determining the synchronous state (see also Ref. [23]). In Ref. [21] for small-world networks of Rössler oscillators, it was shown that the basin stability of the synchronization regime grows rapidly and then exponentially declines as the rewiring probability increases.

In this work we consider small-world networks where the node's oscillators display chaotic spike-burst oscillations, i.e., fast-slow systems, one of the important oscillatory modes in neuron networks. We study the basin stability of the burst synchronization regime depending on topological features, coupling strength, as well as on nodal dynamic properties. In Sec. II the main properties of the nodal dynamics are described, in Sec. III burst synchronization is introduced and the procedure of estimating basin stability is explained. Sections IV and V are devoted to studying the impact of connectivity and nodal dynamics, respectively, on the basin stability of burst synchronization. Finally, in Sec. VI we draw conclusions and discuss our main results.

II. NODAL DYNAMICS

The dynamics of the nodes are described by a discrete-time system [24,25]:

$$\begin{aligned} x_{i,n+1} &= x_{i,n} + F_H(x_{i,n}) - y_{i,n} + I_{i,n}, \\ y_{i,n+1} &= y_{i,n} + \varepsilon(x_{i,n} - J_i), i = 1,...,N. \end{aligned} \tag{1}$$

Here $n = 0,1,2,\ldots$ is discrete time, the variables $x_{i,n}$ and $y_{i,n}$ characterize the state of the ith oscillator at the moment of n. The nonlinear function $F_H(x) = x(x-a)(1-x) - \beta H(x-d)$, where $H(x)$ is the Heaviside step function, and the parameters a, β, and d control the dynamical oscillatory regime. The parameter ε determines the rate for the variable y_i, J_i characterizes the excitatory properties of oscillator i, and the term I_i is an external influence on the ith oscillator. System (1) is constructed from a discrete version of FitzHugh-Nagumo model with an additionally introduced discontinuity expressed by $-\beta H(x-d)$. Depending on parameter values it reproduces a wide range of dynamical regimes displayed by real neurons, for example, excitable regimes, periodic spiking, subthreshold oscillations, spike-bursting, etc. The shape of signals generated is controlled by a, and their period is determined by ε and J_i. The discontinuity term allows one to obtain chaotic regimes that are absent in standard FitzHugh-Nagumo-type systems, namely chaotic spike-burst oscillations. This property is due to the fact that the fast subsystem (i.e., where $\varepsilon = 0$) of the basic model (1) is a Lorenz-type map for certain parameter values. By varying β and d one can modify the amplitude and number of spikes in bursts (for more details, see Refs. [24,25]). An example of chaotic spike-burst behavior generated by Eq. (1) is shown in Fig. 1, where a chaotic attractor and the corresponding waveform are shown in Figs. 1(a) and 1(b),

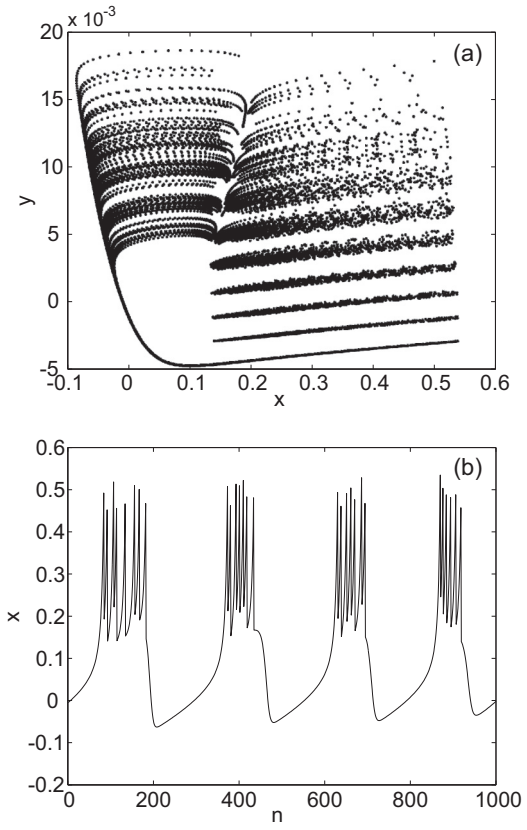

FIG. 1. (a) Chaotic attractor of the single map (1) for $a = 0.1$, $\beta = 0.3$, $d = 0.45$, $\varepsilon = 0.001$, $J = 0.1$, and $I = 0$. (b) Corresponding spike-burst oscillations.

respectively. In this work we deal with oscillators exhibiting such type of activity. Since we study, besides others, the nodal effect on collective phenomena, one should know the properties of individual bursting dynamics such as an average period and number of spikes per burst depending on ε and J_i. Figure 2 shows the average period of spike-burst oscillations, the average duration of the active phase where spikes are generated, and the average number of spikes per burst. Depending on ε and J these characteristics are rather smooth, which indicates that the properties of the chaotic attractor are structurally stable with respect to parameter varying.

Now consider a small-world network of N node's oscillators expressed by Eq. (1) connected with each other by undirected links. The small-world topology is constructed by means of the Watts-Strogatz algorithm [16]. We start with a regular ring-like network where each node is connected to $2k$ neighboring nodes; i.e., the degree of each node is equal to $2k$. Then we look over all existing links and with probability P_{rew} the connection between node i and node j breaks and a new connection is created between node i and another randomly chosen node h. Note that the total number of links (kN) in the network does not change, and the parameter P_{rew} is thus a measure for regularity and randomness of the network topology: $P_{\text{rew}} = 0$ corresponds to a regular network, $P_{\text{rew}} = 1$ corresponds to an absolutely random one, and networks with P_{rew} between 0 and 1 have both features. One of the problems we are interested in is what influence do the topology parameters (P_{rew}, k) have on the synchronization properties of such networks in terms of basin stability.

The internodal interaction expressed by the term I_i in Eq. (1) is modeled by the simplest coupling scheme where the nodes are diffusively connected by the undirected links that have the same coupling strength; i.e., the coupling term reads

$$I_{i,n} = \frac{c}{N}\sum_{j=1}^{N} G_{i,j}(x_{j,n} - x_{i,n}), \quad i = 1,\ldots,N, \qquad (2)$$

where c controls the global coupling strength, and the elements $G_{i,j}$ of the matrix G determine the network topology: $G_{i,j} = 1$ if there is a connection between nodes i and j, and $G_{i,j} = 0$ otherwise.

It should be noted that we consider networks of nonidentical oscillators that have different J_i-values and that are Gaussian distributed with mean J_0 and variance δJ. The waveforms produced by the network dynamics of such oscillators are shown in Fig. 3. It is seen that in a purely regular network [Fig. 3(a)], the spikes of active phases appear in a shifted manner, while in the case of a network with rewired links the spikes emerge in closer instants [Fig. 3(b)].

III. BURST SYNCHRONIZATION AND BASIN STABILITY

A usual way to estimate burst synchronization [13,26,27] is to introduce a phase variable for each oscillator and to compute the complex order parameter in the Kuramoto's sense whose time-averaged magnitude characterizes phase synchronization of bursts [28]. A possible method for defining a phase is to assume the beginning of each burst as a moment for zero phase and during the instants in between the phase increases linearly from zero to one. Obviously for this method one needs to know the oscillation period, which is varying and is unknown *a priori*, and hence it is often difficult to define a phase unambiguously. Here we use an alternative and rather simple method proposed in Refs. [29,30] and developed in Ref. [31], which gives similar results, however, does not require introducing a phase and is based on finding coincident active phases.

The procedure of estimating a burst synchronization degree is the following. Since we deal with nonidentical oscillators having different J_i values, we determine a minimum value of this parameter in the network: $J_{\min} = \min_{i=1\ldots N}\{J_i\}$. We say that the ith oscillator is in an active phase if $x_{i,n} > J_{\min}$, and it is in a passive (or quiescent) phase otherwise. We describe the state of the ith oscillator by the auxiliary variable χ_i, where $\chi_i = 1$ for $x_{i,n} > J_{\min}$ and $\chi_i = 0$ for $x_{i,n} \leqslant J_{\min}$. For a long enough time series $\{x_{i,n}, i = 1\ldots N, n = 0\ldots T\}$, we calculate the following quantity:

$$T_{\text{act}} = \frac{1}{N}\sum_{i=1}^{N}\sum_{n=0}^{T}\chi_{i,n}, \qquad (3)$$

which measures the duration of all active phases averaged over the network. Next, we calculate the quantity

$$T_{\text{coin}} = \sum_{n=0}^{T}\prod_{i=1}^{N}\chi_{i,n}, \qquad (4)$$

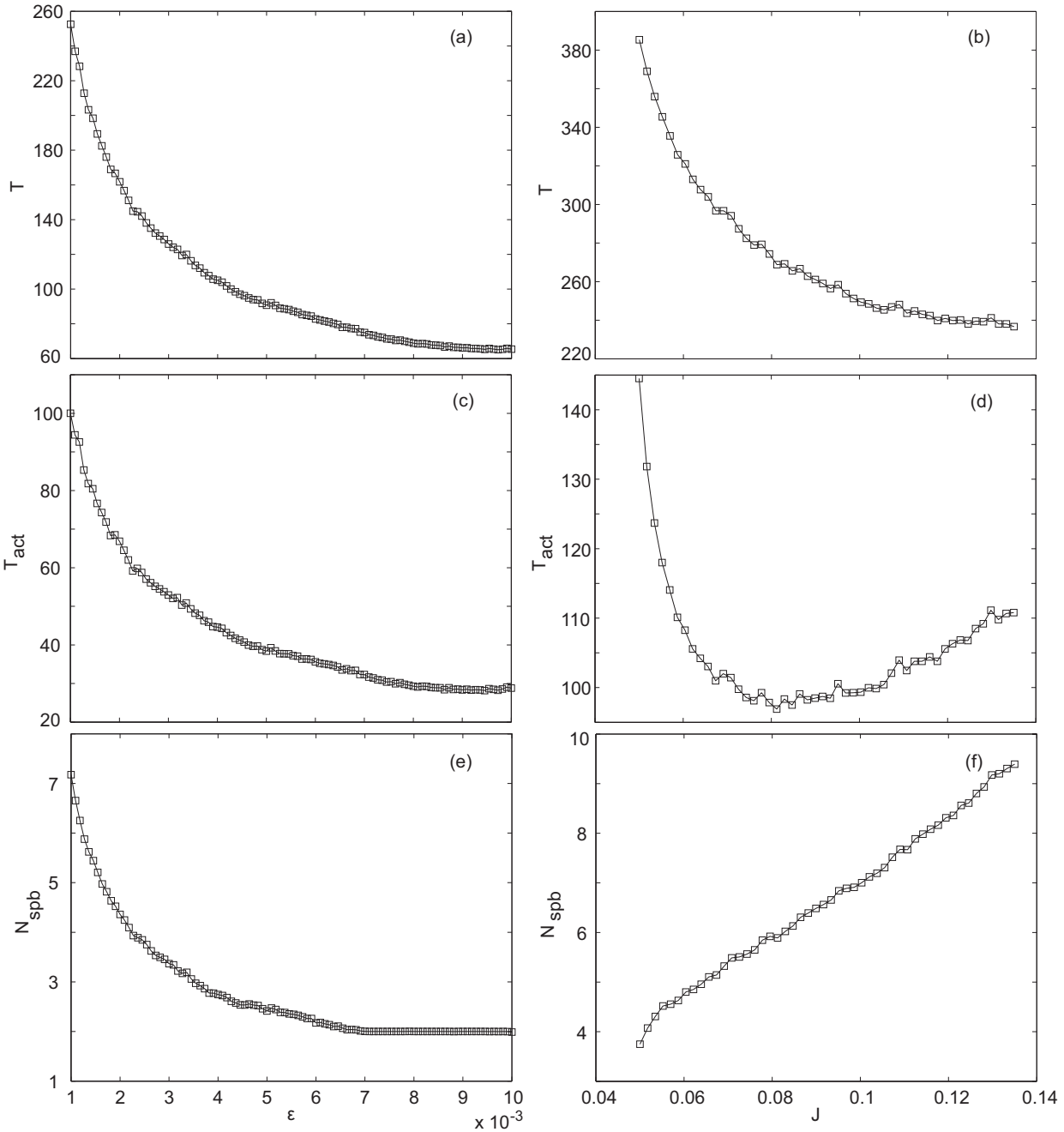

FIG. 2. Properties of chaotic spike-burst oscillations generated by Eq. (1): (a, b) their average period, (c, d) average duration of the active phase, and (e, f) average number of spikes per burst, depending on (a, c, e) ε (for $J = 0.1$) and (b, d, f) J (for $\varepsilon = 0.001$). The other parameters are $a = 0.1$, $\beta = 0.3$, $d = 0.45$, and $I = 0$.

which equals the time during which all the oscillators are simultaneously in an active phase. It is clear that the ratio of these two quantities,

$$\sigma = T_{\text{coin}}/T_{\text{act}}, \tag{5}$$

determines the average fraction of simultaneous generation of active phases in a total duration of all active phases. In other words, σ close to 1 corresponds to burst synchronization when the active phases of different oscillators start and end at close instants of time; the closer σ to 0, the lower the burst synchronization degree is. We compared this method with the phase approach to burst synchronization and found a qualitative similarity of the results they gave (see also Refs. [30,31]).

Basin stability of a synchronization regime gives information about a relative volume of the attraction basin of the attractor corresponding to this regime. By the relative volume of the basin we mean that we do not calculate its absolute value but we quantify it relatively to the phase-space region where the dynamics under study occur after long enough transients. This region is chosen as an area for uniformly distributed initial conditions. Since we deal

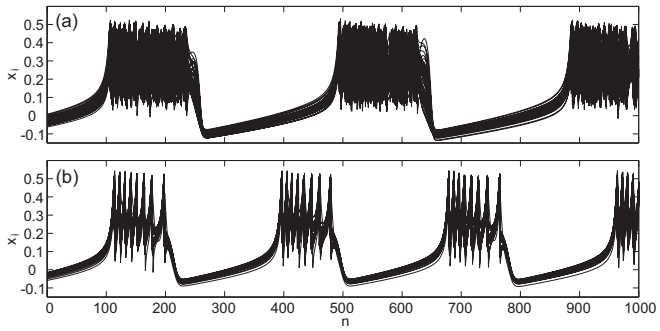

FIG. 3. Burst oscillations in small-world networks of $N = 50$ nodes for different rewiring probabilities: (a) $P_{\text{rew}} = 0$; (b) $P_{\text{rew}} = 0.3$. The other parameters are $c = 1$, $k = 11$, $J_0 = 0.1$, and $\delta J = 0.015$.

with burst synchronization of nonidentical oscillators, it is necessary to define what we mean by a burst synchronization regime. In other words, one should specify a threshold σ_{th} such that when $\sigma > \sigma_{\text{th}}$ then we say that there is the regime of burst synchronization. For time series starting from different initial conditions and (or) different structure configurations one usually obtains various values of σ due to the chaotic dynamics, nonidentity, and topological variability. The distributions of σ's shown in Fig. 4 for different values of ε indicate rather strong differences of the widths as well as the maxima of these curves. The choice of σ_{th} is rather arbitrary, however, as it is seen from Fig. 4 that if one chooses, say, $\sigma_{\text{th}} = 0.95$, then all σ's lie below this value and hence burst synchronization with such a criterion is not reachable for any initial conditions. In most cases we use $\sigma_{\text{th}} = 0.85$, which allows us to monitor changes in the basin stability under varying parameters, and in some cases we discuss what happens if one considers other possibilities (e.g., $\sigma_{\text{th}} = 0.9, 0.8$).

To characterize a relative volume of the attraction basin of the burst synchronization regime, we perform the following procedure. For each set of network parameters we generate M different realizations, and for each of them we compute the value of σ. After that we calculate the number of realizations, M_s, for which $\sigma > \sigma_{\text{th}}$, then the ratio of M_s to M gives an estimation of the basin stability S_B:

$$S_B = M_s/M. \tag{6}$$

Obviously, the value of S_B changes within the interval from 0 to 1; and the closer S_B to 1, the higher the basin stability, and it is more likely that the network comes to the burst synchronous state.

Note that for each of the M realizations, the initial conditions for each oscillator are chosen randomly from a uniform distribution within the area $A = \{-0.12 < x_i < 0.5, -0.005 < y_i < 0.035\}$, $i = 1 \ldots N$, where the chaotic attractor is localized, and moreover, a new network configuration (if there are several of them) is generated for the topology with the same characteristics. Thus, Eq. (6) takes into consideration an averaging over the initial conditions of (x_i, y_i) as well as over the ensemble of different networks with the same topological parameters (N, k, P_{rew}). It should be also noted that when calculating σ, the first T_0 values of $x_{i,n}$ are skipped, and the remained $T - T_0$ ones are taken.

IV. IMPACT OF CONNECTIVITY PARAMETERS

First, we examine the impact of the network connectivity on the collective dynamics; i.e., we are interested in the role of the rewiring probability P_{rew}, the nodal degree k, and the coupling strength c. Figure 5 shows $S_B(P_{\text{rew}})$ for different small values of the parameter ε. One can see that three of the curves have rather steep increasing parts below some critical value P^*_{rew} and flat decreasing parts above P^*_{rew}. The other two curves are considerably lower than the previous three; however, one can distinguish similar but less pronounced increasing and decreasing parts. These features of $S_B(P_{\text{rew}})$ are qualitatively similar to the case of small-world networks of Rössler oscillators in the sense that the curves have a maximum

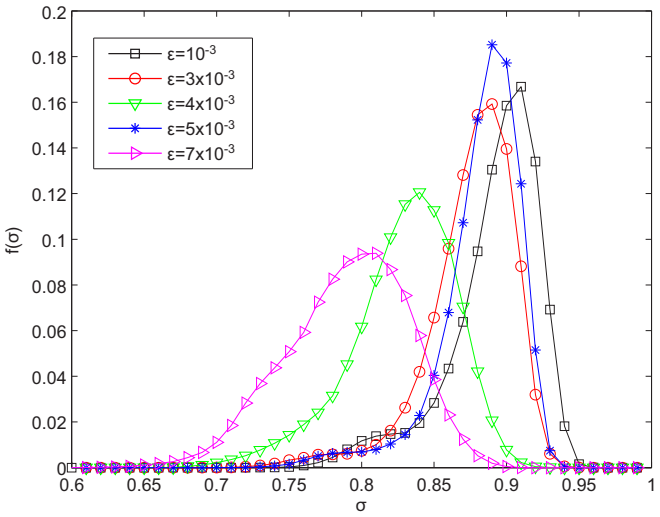

FIG. 4. (Color online) Distribution of σ values for different ε values. The parameters are $N = 50$, $P_{\text{rew}} = 0.3$, $k = 11$, $c = 1$, $J_0 = 0.1$, and $\delta J = 0.01$.

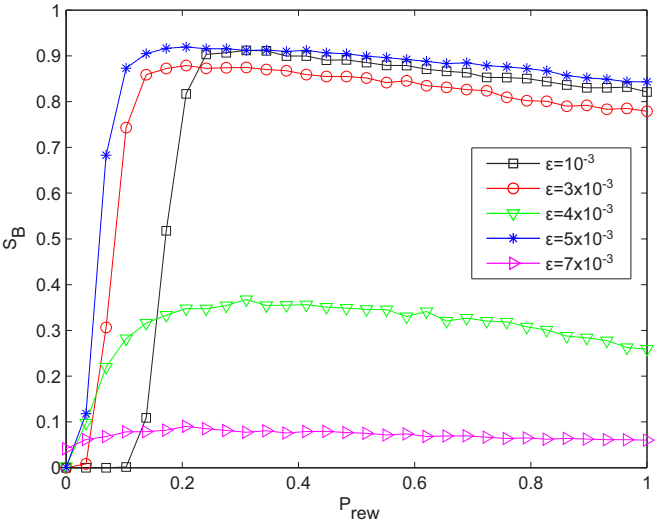

FIG. 5. (Color online) Basin stability versus rewiring probability P_{rew} for different values of ε. The parameters are $N = 50$, $k = 11$, $c = 1$, $J_0 = 0.1$, and $\delta J = 0.01$.

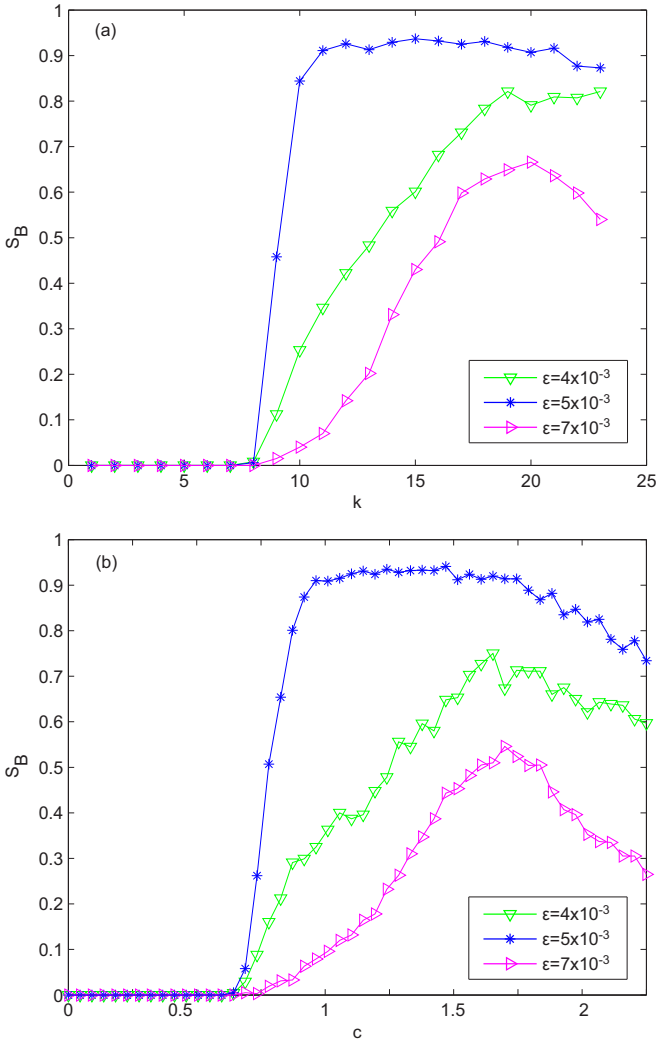

FIG. 6. (Color online) Basin stability versus (a) degree k (for $c = 1$) and (b) coupling strength c (for $k = 11$) for different values of ε. The parameters are $N = 50$, $P_{\text{rew}} = 0.3$, $J_0 = 0.1$, and $\delta J = 0.01$.

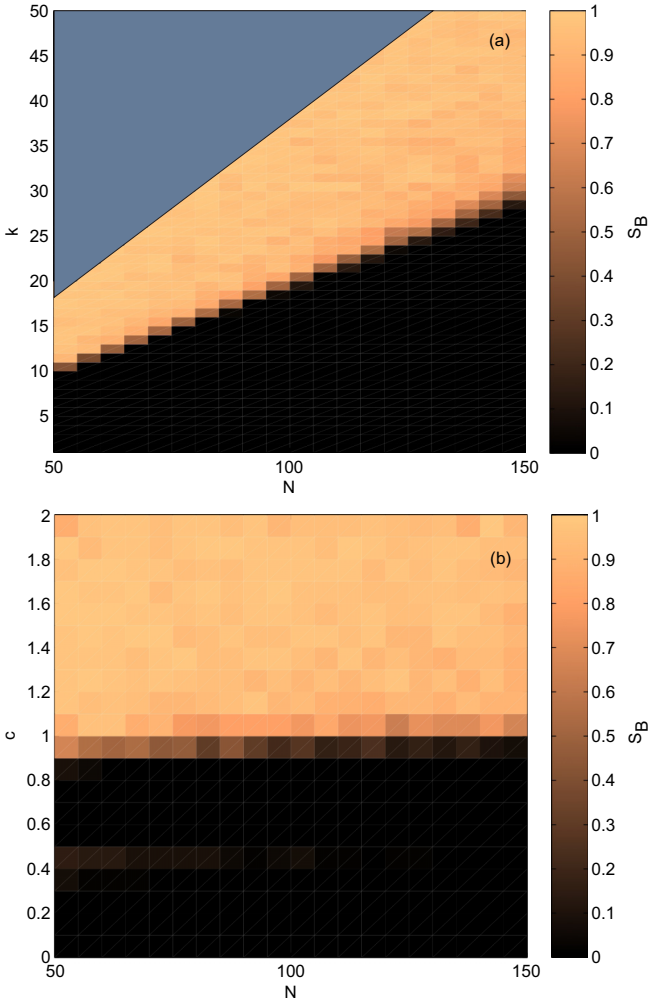

FIG. 7. (Color online) Basin stability versus (a) N and k (for $c = 1$) and (b) N and c (for $k = 0.2 \times N$). The parameters are $J_0 = 0.1$, $\delta J = 0.01$, $\varepsilon = 10^{-3}$, $P_{\text{rew}} = 0.3$.

corresponding to the rewiring probability providing the largest basin stability. However, an important distinction in our case is that the decay of $S_B(P_{\text{rew}})$ is not exponential, but it is close to linear and there are no such pronounced peaks in the curves like in Rössler networks. So there are rather wide intervals of P_{rew} for which S_B takes its maximum value. Note that the curves are sensitive to the nodal parameter ε. In particular, the maximum of basin stability for $\varepsilon = 10^{-3}$ is much larger than that for $\varepsilon = 4 \times 10^{-3}$; the curve for $\varepsilon = 5 \times 10^{-3}$ is above that for $\varepsilon = 4 \times 10^{-3}$ for all rewiring probabilities, and the threshold for reaching a maximum in the case of $\varepsilon = 5 \times 10^{-3}$ is lower than that for $\varepsilon = 10^{-3}$. Below we consider in more detail the influence of nodal dynamics on the basin stability of burst synchronization.

The next question is the influence of the network density characterized by k. Figure 6(a) shows that for very sparse networks the burst synchronous regime has a basin stability near zero. Only above some threshold value of k, the basin stability begins to grow rapidly. An important point is that for very dense networks [see $k > 20$ in Fig. 6(a)] S_B begins to decrease. With increasing number of links in the network (while the other parameters are fixed), the coupling term I_i in system (1) grows, the spike-burst oscillations are distorted, and there appear outbursts from active chaotic phases to passive ones. According to our criterion of burst synchronization, this means that the duration of simultaneous generation of bursts decreases; hence, σ also decreases and the synchronous state may not be reached.

An analogous effect is observed for increasing coupling strengths [see Fig. 6(b)]. In all the cases, there is a threshold value of c above which S_B gradually increases and reaches its maximum value. Note that when the coupling strength becomes sufficiently large, the basin stability decreases, which occurs due to the same factors as previously discussed for the effect of k. The larger c, the greater the coupling term, and starting from some c there is a distortion of bursts, and for a further increase of the coupling strength [not shown in Fig. 6(b)], the coupling term I_i can be so large that individual oscillators leave the partial chaotic attractors and go to infinity.

We checked these effects depending on the network size and found that for $N = 50 \div 150$, the transition from low to

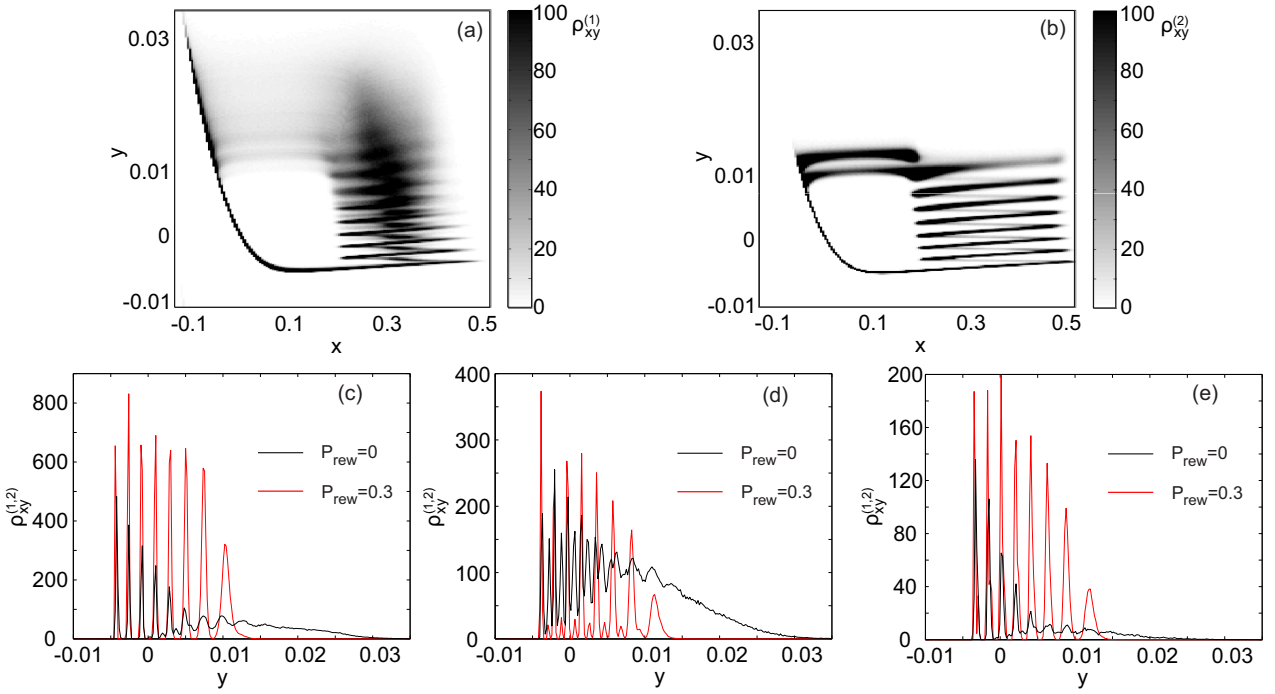

FIG. 8. (Color online) Probability distribution $\rho_{x,y}$ in phase plane (x,y) of the trajectories $(x_{\text{mean}},y_{\text{mean}})$ averaged over the network for (a) $P_{\text{rew}}=0$ and (b) $P_{\text{rew}}=0.3$ (for $N=50$, $k=11$, $c=1$, $J_0=0.1$, and $\delta J=0.01$). Projections of these distributions on line (c) $x=0.2$, (d) $x=0.3$, and (e) $x=0.4$.

high basin stability occurs near $k\approx 0.2N$ for a wide range of parameters [an example is shown in Fig. 7(a)], while in terms of the coupling strength this occurs at about $c=1.0$ [Fig. 7(b)].

In order to relate a deformation of phase-space geometry with network rewiring, we study probability density distributions. We explore the motion of trajectories $(x_{\text{mean}}, y_{\text{mean}})$ in the phase plane (x,y), where $x_{\text{mean}}=\frac{1}{N}\sum_{j=1}^{N}x_j$, $y_{\text{mean}}=\frac{1}{N}\sum_{j=1}^{N}y_j$. Similarly to the procedure described in Sec. III, we compute time series of $(x_{\text{mean}}, y_{\text{mean}})$ for M different realizations that characterize a certain network structure. We place a partition grid with rectangles $R_{x,y}$ with sizes $\Delta x\times\Delta y$ onto the region A and compute how often phase points fall into each $R_{x,y}$. The ratio of the number of points $N_{x,y}$ in a rectangle $R_{x,y}$ to the total number of points $M\times T$ (where T is the duration of time series) gives an estimate of the probability for a trajectory to enter $R_{x,y}$. We define the probability density as $\rho_{x,y}=N_{x,y}/(MT\Delta x\Delta y)$ and plot this for different networks comparing with corresponding values of basin stability. Figures 8(a) and 8(b) show $\rho_{x,y}$ for two different rewiring probabilities $P_{\text{rew}}=0$ (a regular network) and $P_{\text{rew}}=0.3$ (a small-world network). These distributions have some similarities with the chaotic attractor of an individual oscillator [cf. Fig. 1(a)], e.g., they have a left-hand branch of slow regular motions and a right-hand region of fast chaotic motions. However, the distributions $\rho^{(1)}_{x,y}$ in Fig. 8(a) and $\rho^{(2)}_{x,y}$ in 8(b) differ from each other in some key points. First, the distribution $\rho^{(2)}_{x,y}$ has more distinct stripes in the chaotic region which correspond to phase-space regions with the most likely trajectory visiting. This is supported by Figures 8(c), 8(d), and 8(e), which show projections of $\rho^{(1,2)}_{x,y}$ onto different vertical lines. Second, the distribution corresponding to $P_{\text{rew}}=0$ has wider sizes in the y direction of its regular and chaotic parts compared to that of the case $P_{\text{rew}}=0.3$. Since Fig. 8(b) corresponds to the case with the highest basin stability, those phase trajectories that move mainly in $\rho^{(2)}_{x,y}$ determine the regime of burst synchronization according to the definition given in Sec. III. Note that in the case of $\rho^{(1)}_{x,y}$, trajectories spend a long time moving in an upper area that is beyond $\rho^{(2)}_{x,y}$, and hence these trajectories do not contribute to the burst synchronization regime and the respective basin stability is close to zero. Comparing a distribution $\rho_{x,y}$ corresponding to some network topology with $\rho^{(2)}_{x,y}$, one can conclude whether this topology results in a high basin stability for burst synchronization (if $\rho_{x,y}$ is similar to $\rho^{(2)}_{x,y}$) or in low one (if $\rho_{x,y}$ is close to $\rho^{(1)}_{x,y}$).

V. IMPACT OF NODAL PARAMETERS

The next important question is about the influence of nodal dynamics on the basin stability. An interesting problem is what are the consequences of a change in the properties of the chaotic attractor controlled by the parameters ε and J_0. As it follows from the previous section, the parameter ε has a drastic impact on the basin stability (see Fig. 5). Now for the fixed connectivity parameters $P_{\text{rew}}=0.3$ and $k=11$ and the coupling strength $c=1$ we plot S_B versus ε for $J_0=0.1$. Figure 9 (black squares) shows several pronounced maxima and minima of $S_B(\varepsilon)$, e.g., two maxima at $\varepsilon=3\times10^{-3}$ and $\varepsilon=5\times10^{-3}$ and the minima at $\varepsilon=4\times10^{-3}$ and $\varepsilon=8\times10^{-3}$ (compare with Fig. 5). Note that in Fig. 9 shown are also curves obtained for other burst synchronization criteria

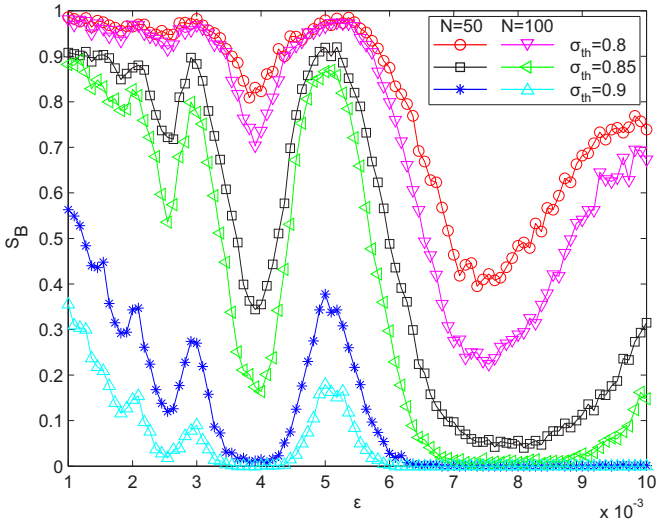

FIG. 9. (Color online) Basin stability versus ε. The influence of σ_{th} and network size N are shown. For the case of $N = 50$, $k = 11$; for the case of $N = 100$, $k = 22$. In all the cases $P_{\rm rew} = 0.3$, $c = 1$, $J_0 = 0.1$, and $\delta J = 0.01$.

$\sigma_{\rm th}$ (red circles for $\sigma_{\rm th} = 0.8$ and blue asterisks for $\sigma_{\rm th} = 0.9$). These two curves repeat the main properties of the first one (corresponding to $\sigma_{\rm th} = 0.85$), i.e., qualitatively indicate the existence of ε values corresponding to low or high basin stabilities. One can see that the greater $\sigma_{\rm th}$, the less S_B, i.e., a less number of initial conditions come to the burst synchronous state defined by the particular $\sigma_{\rm th}$ criterion.

We studied the effect of the network size and found that the important properties of the basin stability remain the same for larger networks. Figure 9 shows that for $N = 100$ the curves shown by triangles for different $\sigma_{\rm th}$ criteria are very similar to those corresponding to $N = 50$. They have their maxima and minima at the same values of ε; however, for most of ε's, the basin stability of the larger network is lower than that for the smaller ones.

Another nodal parameter J_0 also controls the basin stability as it follows from Fig. 10(a), which shows S_B versus J_0 for three different values of ε. While for $\varepsilon = 10^{-3}$ the basin stability gradually increases from small values and becomes close to one, for the other two ε's we observe oscillatory curves $S_B(J_0)$. It is interesting to note that changing ε from 4×10^{-3} just to 5×10^{-3}, the J_0 coordinates for maxima and minima of the basin stability are shifted.

It should be noted that the influence of the parameter δJ as a measure of similarity is to decrease basin stability S_B with increasing δJ as shown in Fig. 10(b). The figure demonstrates that identical nodes as well as those with small enough mismatch tend to have a larger basin stability for burst synchronization than that of strongly mismatched nodes.

To understand the reason for the intricate behavior of S_B versus J_0, we plot the characteristics of burst oscillations, the average number of spikes per burst $N_{\rm spb}$, and the average duration of the active phase $T_{\rm act}$. Both quantities are averaged over time and over all oscillators, i.e., they take into account the joint effect of nodal dynamics and internodal complex interaction. Figure 11 shows for two different ε's the dependence of $N_{\rm spb}$

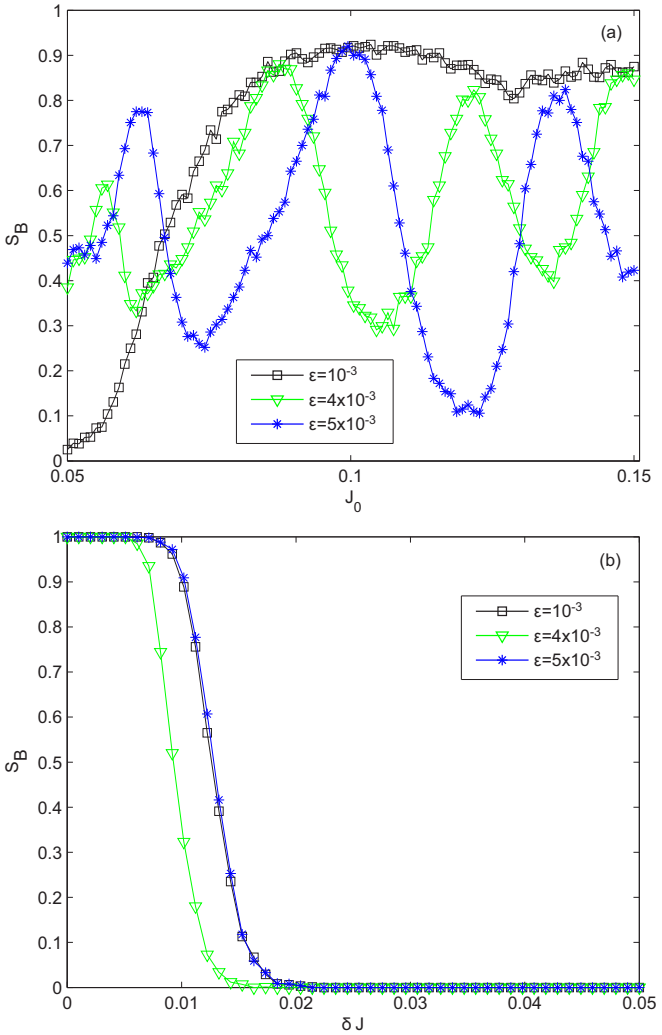

FIG. 10. (Color online) Basin stability versus (a) J_0 (for $\delta J = 0.01$) and (b) δJ (for $J_0 = 0.1$) for different values of ε. The parameters are $N = 50$, $P_{\rm rew} = 0.3$, $k = 11$, $c = 1$.

and $T_{\rm act}$ on J_0, and by comparing these plots with $S_B(J_0)$, we find that the local maxima of the $T_{\rm act}(J_0)$ appear near the same values of J_0 as the local maxima of $S_B(J_0)$, and at these J_0's the average number of spikes per burst changes abruptly. Hence, the curves $N_{\rm spb}(J_0)$ have a stair-like form. These facts mean that the local increases of the basin stability are associated with increasing active burst phases and, at the same time, with the appearing of new spikes in the bursts.

Note that such characteristic as the average number of spikes per burst calculated for individual nodal dynamics, depends monotonically on J; namely, in the region shown in Fig. 11 individual $N_{\rm spb}$ increases monotonically with increasing J (see Fig. 2(f)). However, if one considers another quantity of individual nodal dynamics, the most likely value of the number of spikes per burst, it has a stair-like form analogous to those shown in Figs. 11(c) and 11(d). One can conclude that the collective network effect, among others, is to make the distributions more symmetric and, as a result, to transform most likely characteristics to averaged ones. To compare the network effect with individual dynamic features,

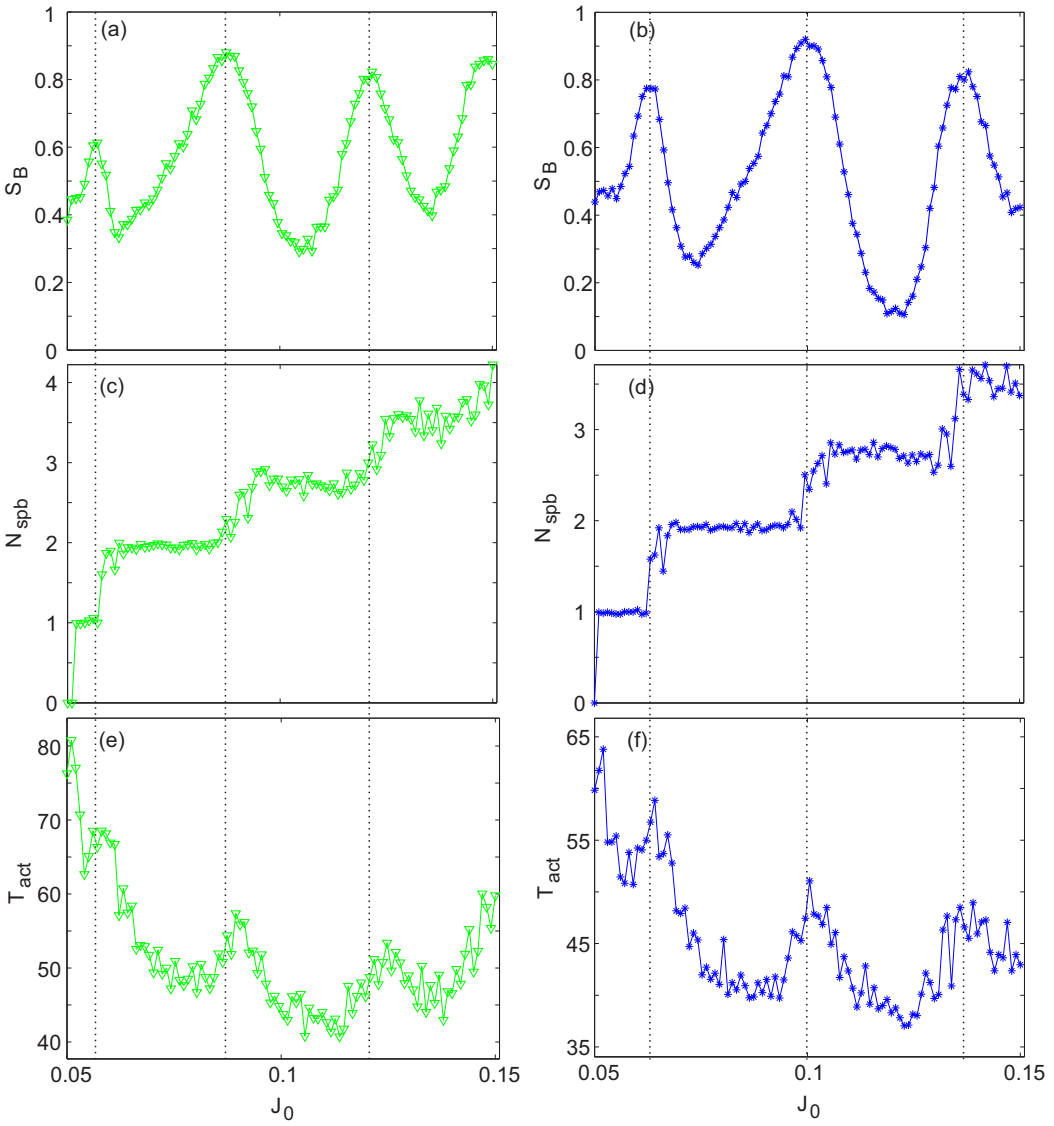

FIG. 11. (Color online) (a, b) Basin stability, (c, d) average number of spikes per burst, and (e, f) average duration of the active phase versus J_0 for different values of ε: $\varepsilon = 0.004$, left, and $\varepsilon = 0.005$, right. The parameters are $N = 50$, $P_{\text{rew}} = 0.3$, $k = 11$, $c = 1$, and $\delta J = 0.01$.

we plot S_B versus ε and J_0 (see Fig. 12) and show the curves which divide the (ε, J_0) plane into regions where a single oscillator with corresponding parameters generates bursts with the most probable value of N_{spb} indicated in the plane by numbers 1 . . . 10. It is seen that in general the borders between different areas fall onto the local maxima of the basin stability, however, this is not the case for small ε's, in particular $\varepsilon < 2 \times 10^{-3}$.

VI. CONCLUSION

We have studied properties of burst synchronization in small-world networks of map-based chaotic neurons in terms of basin stability. With increasing rewiring probability the basin stability of the burst synchronization regime first sharply increases, reaches its maximum value, and then gradually decreases. The problem of stability of synchronization regimes in neural networks has a particular meaning as far as in large-scale complex neural circuits there are usually a variety of possible oscillatory modes, and it is very important to know how robust is a certain regime to external perturbations [32,33]. In particular, since most of neural networks are adaptive systems in which the connectivity structure can evolve along with cellular and synaptic dynamics, one has to study the impact of topology rewiring on collective behavior. The framework of basin stability has already allowed us to uncover important mechanisms of dynamical networks' behavior. In Ref. [34] the authors showed that changes of basin of attraction of the synchronization state underlies a hysteretic behavior at the transition to synchronization. The authors of Ref. [35] found that in networks with stochastically rewired links the small-world topology leads to the largest sensitivity to dynamic connections, i.e., the basin stability of the synchronization regime in small-world networks starts to increase at lower rewiring frequencies than that of random ones.

We have considered small-world networks containing a few dozens oscillators, which is certainly not the case for large-scale biological neural networks. However, in many

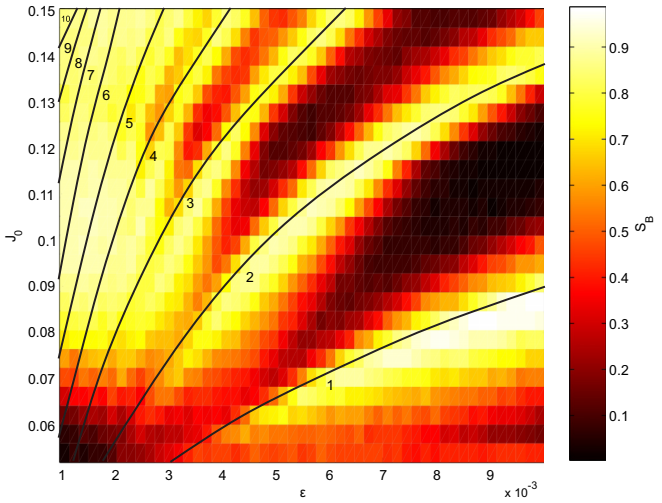

FIG. 12. (Color online) Basin stability versus ε and J_0. The parameters are $N = 50$, $P_{\text{rew}} = 0.3$, $k = 11$, $c = 1$, and $\delta J = 0.01$. The solid curves divide the plane into areas with different numbers of spikes per bursts indicated on the plot by $1 \ldots 10$.

experimental *in vitro* studies neural cultures evolve to a multicluster state where each densely packed cluster comprises about one hundred cells (see, e.g., Ref. [36]). Our result suggests that there is an optimal ratio between regular and random features of the network structure corresponding to the largest basin of stability of the burst synchronization state. Another point is that unlike the networks of Rössler oscillators, the basin stability remains relatively large if one increases randomness in a network topology, i.e., bursting oscillators display synchronization that is more reliable to rewiring in the sense of basin stability.

We have also found that the coupling density and the coupling strength influence the basin stability similarly, i.e., they have some threshold values, below which the burst synchronization regime is hardly reachable, and above which the basin stability grows up. Normally, the basin stability slightly decreases with increasing coupling density or strength for relatively large values of them. An intriguing dependence of the basin stability on the parameters of individual nodal dynamics is observed; i.e., there is a possibility to get either small or large basin stability in the same network by only varying the parameters of relaxation or excitability. We have explained this effect revealing that the number of spikes per burst plays a key role in such a collective phenomenon. We have also discussed the impact of the network size and the criterion of burst synchronization chosen.

An interesting point is that although we have considered bursting oscillators and applied the specific synchronization criterion we have found that the rewiring of links influences the basin stability in a manner similar to small-world networks of identical Rössler oscillators [21]. This result suggests the generality of the effect in a quite wide class of complex oscillatory networks. However, it is still needed to investigate other kinds of oscillators and other types of synchronization. Our calculation confirmed the usage of the basin stability approach as the most convenient way to explore synchronization phenomena in large-scale systems where other methods are hardly applicable due to nonidentical elements.

ACKNOWLEDGMENTS

This work was supported by the Government of the Russian Federation (Agreement No. 14.Z50.31.0033 with the Institute of Applied Physics of RAS).

[1] E. M. Izhikevich, *Dynamical Systems in Neuroscience: The Geometry of Excitability and Bursting* (The MIT Press, Cambridge, 2007).
[2] R. Albert and A.-L. Barabási, Statistical mechanics of complex networks, Rev. Mod. Phys. **74**, 47 (2002).
[3] M. E. Newman, The structure and function of complex networks, SIAM Rev. **45**, 167 (2003).
[4] S. H. Strogatz, Exploring complex networks, Nature **410**, 268 (2001).
[5] S. Boccaletti, V. Latora, Y. Moreno, M. Chavez, and D.-U. Hwang, Complex networks: Structure and dynamics, Phys. Rep. **424**, 175 (2006).
[6] A. B. Neiman and D. F. Russell, Synchronization of Noise-Induced Bursts in Noncoupled Sensory Neurons, Phys. Rev. Lett. **88**, 138103 (2002).
[7] I. Belykh, E. de Lange, and M. Hasler, Synchronization of Bursting Neurons: What Matters in the Network Topology, Phys. Rev. Lett. **94**, 188101 (2005).
[8] N. F. Rulkov, Regularization of Synchronized Chaotic Bursts, Phys. Rev. Lett. **86**, 183 (2001).
[9] X. Lang, Q. Lu, and J. Kurths, Phase synchronization in noise-driven bursting neurons, Phys. Rev. E **82**, 021909 (2010).
[10] S. Liepelt, J. A. Freund, L. Schimansky-Geier, A. Neiman, and D. F. Russell, Information processing in noisy burster models of sensory neurons, J. Theoret. Biol. **237**, 30 (2005).
[11] A. Pikovsky, M. Rosenblum, and J. Kurths, *Synchronization: A Universal Concept in Nonlinear Sciences*, Vol. 12 (Cambridge University Press, Cambridge, 2003).
[12] G. V. Osipov, J. Kurths, and C. Zhou, *Synchronization in Oscillatory Networks* (Springer, Berlin, 2007).
[13] C. A. S. Batista, E. L. Lameu, A. M. Batista, S. R. Lopes, T. Pereira, G. Zamora-Lopez, J. Kurths, and R. L. Viana, Phase synchronization of bursting neurons in clustered small-world networks, Phys. Rev. E **86**, 016211 (2012).
[14] M. Dhamala, V. K. Jirsa, and M. Ding, Transitions to Synchrony in Coupled Bursting Neurons, Phys. Rev. Lett. **92**, 028101 (2004).
[15] Y. Shen, Z. Hou, and H. Xin, Transition to burst synchronization in coupled neuron networks, Phys. Rev. E **77**, 031920 (2008).
[16] D. J. Watts, S. H. Strogatz, Collective dynamics of "small-world" networks, Nature **393**, 440 (1998).
[17] D. J. Watts, *Small Worlds* (Princeton University Press, Princeton, 1999).

[18] C. J. Stam and J. C. Reijneveld, Graph theoretical analysis of complex networks in the brain, Nonlin. Biomed. Phys. **1**, 3 (2007).

[19] E. Bullmore, O. Sporns, Complex brain networks: Graph theoretical analysis of structural and functional systems, Nat. Rev. Neurosci. **10**, 186 (2009).

[20] G. Gong, Y. He, L. Concha, C. Lebel, D. W. Gross, A. C. Evans, C. Beaulieu, Mapping anatomical connectivity patterns of human cerebral cortex using in vivo diffusion tensor imaging tractography, Cereb. Cortex **19**, 524 (2008).

[21] P. J. Menck, J. Heitzig, N. Marwan, and J. Kurths, How basin stability complements the linear-stability paradigm, Nature Phys. **9**, 89 (2013).

[22] P. J. Menck, J. Heitzig, J. Kurths, and H. Joachim Schellnhuber, How dead ends undermine power grid stability, Nat. Commun. **5**, 3969 (2014).

[23] D. A. Wiley, S. H. Strogatz, and M. Girvan, The size of the sync basin, Chaos **16**, 015103 (2006).

[24] V. I. Nekorkin, L. V. Vdovin, Diskretnaya model neyronnoy aktivnosti (Discrete model of neural activity), Izv. Vyssh. Uchebn. Zaved. Prikladn. Nelineyn. Din. **15**, 36 (2007) (in Russian).

[25] M. Courbage, V. I. Nekorkin, L. V. Vdovin, Chaotic oscillations in a map-based model of neuronal activity, Chaos **17**, 043109 (2007).

[26] K. Josić and D. J. Mar, Phase synchronization of chaotic systems with small phase diffusion, Phys. Rev. E **64**, 056234 (2001).

[27] T. Pereira, M. S. Baptista, and J. Kurths, Phase and average period of chaotic oscillators, Phys. Lett. A **362**, 159 (2007).

[28] Y. Kuramoto, *Chemical Oscillations, Waves and Turbulence* (Dover, New York, 2003).

[29] V. I. Nekorkin and O. V. Maslennikov, Spike-burst synchronization in an ensemble of electrically coupled discrete model neurons, Radiophys. Quant. Electron. **54**, 56 (2011).

[30] M. Courbage, O. V. Maslennikov, and V. I. Nekorkin, Synchronization in time-discrete model of two electrically coupled spike-bursting neurons, Chaos, Solitons & Fractals **45**, 645 (2012).

[31] O. V. Maslennikov, V. I. Nekorkin, Modular networks with delayed coupling: Synchronization and frequency control, Phys. Rev. E **90**, 012901 (2014).

[32] G. Deco, V. Jirsa, and K. J. Friston, The dynamical and structural basis of brain activity, in *Principles of Brain Dynamics: Global State Interactions*, edited by M. I. Rabinovich, K. J. Friston, and P. Varona (The MIT Press, Cambridge, 2012).

[33] M. Diesmann, M. O. Gewaltig, A. Aertsen, Stable propagation of synchronous spiking in cortical neural networks, Nature **402**, 529 (1999).

[34] Y. Zou, T. Pereira, M. Small, Z. Liu, and J. Kurths, Basin of Attraction Determines Hysteresis in Explosive Synchronization, Phys. Rev. Lett. **112**, 114102 (2014).

[35] V. Kohar, P. Ji, A. Choudhary, S. Sinha, and J. Kurths, Synchronization in time-varying networks, Phys. Rev. E **90**, 022812 (2014).

[36] S. Teller, C. Granell, M. De Domenico, J. Soriano, S. Gómez, and A. Arenas, Emergence of assortative mixing between clusters of cultured neurons, PloS Comput. Biol. **10**, 1003796 (2014).